SPIN
Vol. 1, No. 1 (2011) 1–4
©World Scientific Publishing Company

Magnetoresistance of nanoscale domain walls formed in arrays of parallel nanowires

Jingchun Wang
School of Physics, Beijing Institute of Technology,
Beijing 100081, P. R. China
Beijing No. 4 High School
Beijing 100034, P. R. China

Floriano Cuccureddu
School of Physics and CRANN, Trinity College Dublin
Dublin 2, Ireland

Rafael Ramos
School of Physics and CRANN, Trinity College Dublin
Dublin 2, Ireland

Cormac Ó Coileáin
School of Physics, Beijing Institute of Technology,
Beijing 100081, P. R. China
School of Physics and CRANN, Trinity College Dublin
Dublin 2, Ireland

Igor V. Shvets
School of Physics and CRANN, Trinity College Dublin
Dublin 2, Ireland

Han-Chun Wu
School of Physics, Beijing Institute of Technology,
Beijing 100081, P. R. China
wuhc@bit.edu.cn

Received Day Month Year
Revised Day Month Year

We present the possibility of enhancing magnetoresistance by controlling nanoscale domain wall (DW) width in a planar nanowire array. Results based on the micromagnetic calculations show that DW width decreases with increasing exchange bias field and decreases with reducing exchange interaction between neighboring nanowires. Fe/Fe_3O_4 nanowire arrays were grown on *c*-plane sapphire to demonstrate the feasibility of this concept, and an enhanced MR ratio of 3.7% was observed at room temperature.

Keywords: A list of 3–5 keywords are to be supplied.

SPIN
Vol. 1, No. 1 (2011) 1–4
©World Scientific Publishing Company

1. Introduction

Nanowires with the dimensions of 10 nm and smaller have great promise for electronic devices of the future. Yet, there are fundamental and practical challenges to be overcome to fulfill their potential. Compared to the areas of organic or semiconductor nanowires, the area of magnetic nanowires is largely undeveloped. There are theoretical proposals of spin-electronic devices utilizing magnetic nanowires, e.g.[1] and there are theoretical treatments of magnetoresistance (MR) in a configuration where the current flows through a single nanowire, e.g.[2]. There are also experimental studies on MR in single nanowires. Typically in these studies the nanowire is formed by means of a top-down lithographic process, meaning that its dimension is relatively large and also the current is driven along the nanowire[3]. The other configuration where the current flows in between nanowires, is highly interesting provided that the magnetization in neighboring nanowires can be controlled independently. In this configuration new device architectures could be expected. It allows for the insertion of the largest possible number of domain walls (DWs) in the current's pathway. Furthermore, the DW separating two nanowires with opposite magnetization directions could be fundamentally different to a conventional DW. The origin of DW resistance is attributed to the mixing of up and down-spin electrons due to the mis-tracking of the electrons' spins on passing through the DW[4]. A narrower DW width results in a larger angle between the magnetization directions of successive atomic layers thereby lowering the electron transmission and hence enhancing the MR. In the ballistic regime, the value of MR as a function of the DW width (d_{DW}) is determined by the electron Fermi wavelength λ_F. In bulk ferromagnets the DW width is entirely determined by the exchange and magnetic anisotropy energies and is typically $d_{DW} \sim 100$ nm, whereas $\lambda F \sim 0.5$ nm. Hence, conventional DWs do not appreciably affect the resistance of bulk ferromagnets because an electron can adiabatically follow the varying magnetization direction within the DW. This behavior could change dramatically in magnetic nanostructures, where the reduced dimensions affect both the DW width and the mechanism of electron transport responsible for the DW resistance. Several theoretical studies[5-7] have been performed on this problem and there is still a debate as to the origin of DW width-dependent magnetoresistance[8]. One such theory suggests that if the DW width is of the order of the Fermi wavelength, λF, then ballistic transport dominates with strong electron reflection from the interface[9]. This is predicted to lead to large MR of a few hundred percent. Effectively, the thinner the DW the larger is the MR. These results are in line with another recent theoretical study[10] that dealt specifically with DWs in magnetic nanowires. Recently, we proposed the concept of nanowire array MR device[11] based on the capabilities of Atomic Terrace Low Angle Shadowing (ATLAS) technique[12]. The ATLAS technique relies on the shadowing that vicinal treated substrates can provide at shallow angle deposition due to the terrace-and-step morphology. It was also demonstrated by Kronmuller *et al* that planar phase boundaries in magnetic materials are found to act as strong repulsive or trapping barriers for the displacement of DWs if the magneto crystalline anisotropies of the two phases are different from each other[13].

In this paper, based on micromagnetic calculations, we first present the possibility of DW width decreasing with exchange bias field and the exchange interaction between the neighboring nanowires in a planar nanowire array. We then present an experimental demonstration using a Fe/Fe_3O_4 nanowire array produced by the ATLAS technique. An enhanced MR ratio of ~4% was observed at room temperature. Our MR measurements illuminate the feasibility of the concept of a nanowire array magnetoresistance device.

2. Theoretical Simulation

The structure studied here consists of a planar array of nanowires (Fig. 1). It relies on the architecture of a recently proposed new magnetoresistive device [11,12]. Two types of nanowires are used: so-called spacer nanowires of insulating or semiconductor material marked orange and so-called magnetoresistive nanowires of e.g. Fe or Co marked grey. The substrate is of an antiferromagnetic single crystal, e.g. NiO. The prime purpose of the spacer nanowires is to destroy exchange coupling between the substrate and one subset of the magnetoresistive nanowires. More details about the structure, as well as other material configurations within the same device architecture, can be found elsewhere[11]. Since the magnetoresistive nanowires of the second subset are exchange-coupled to the antiferromagnetic substrate, these two types of nanowires have different coercivity. Therefore, as a

magnetic field is applied it should be possible to switch between two configurations, in which the magnetoresistive nanowires of the two subsets are either magnetized antiparallel or parallel with respect to each other (Fig. 1(a) and 1(b) respectively). A DW is formed when the neighboring magnetoresistive nanowires are magnetized in an antiparallel configuration. The micromagnetic model includes six types of energy terms: exchange energy (E_{exch}), anisotropy energy (E_{anis}), magnetostatic energy (E_{demag}), Zeeman energy (E_{zeeman}), exchange bias field energy (E_{xcB}) introduced to the pinned nanowires, and the inter-wire exchange coupling energy (E_F) between the neighboring pinned and unpinned nanowires. The magnetic free energy per unit volume is given by

$$e_T = e_{exch} + e_{anis} + e_{demag} + e_{zeeman} + e_{xcB} + e_F \,. \quad (1)$$

Details of the first four energy terms can be found elsewhere[13] and all the parameters in this model, such as value of A (exchange stiffness), can be estimated from experiments or using constrained density functional theory for spin spiral magnetic configurations[14]. The exchange bias field energy e_{xcB} is defined by:

$$H_{xcB} = -\mu_0 \mathrm{M} \cdot H_{\mathrm{xcB}} \cdot \vec{n}, \quad (2)$$

where H_{xcB} is the exchange bias field introduced to the pinned nanowires. This term represents a unidirectional anisotropy introduced by setting bias direction ($\vec{n}$) via field cooling process. The strength of the interwire exchange coupling between the neighboring pinned and unpinned nanowires e_F was modeled by varying boundary exchange stiffness. In order to study the DW "motion" due to the applied field, Landau-Lifshitz-Gilbert (LLG) equation was used and having the following expression[15]:

$$\frac{\partial M}{\partial t} = -\gamma M \times H_{eff} - \frac{\gamma\alpha}{|M|} M \times (M \times H_{eff}),. \quad (3)$$

where the first term is the gyroscopic reaction of the angular momentum associated with the magnetization with an effective field.

$$H_{eff} = -\frac{1}{\mu}\frac{\partial E_T}{\partial M} \quad (4)$$

The magnetization will tend to precess around the field and the coefficient γ is the gyromagnetic ratio. The second term is the one that dissipates energy and the dimensionless α is called the damping coefficient. Most materials have the value α in the range of 0.004 to 0.15. This term is introduced phenomenologically in order to get the system to settle down into an equilibrium state instead of precessing endlessly.

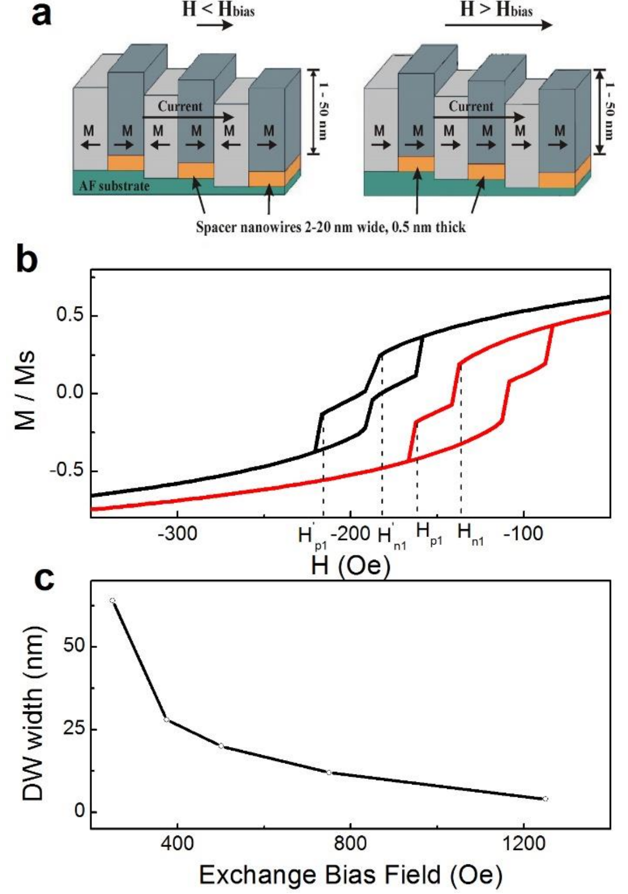

Fig. 1. (Color online) (a) Schematic of nanowire array showing magnetization of the nanowires in antiparallel configuration and parallel configuration. (b) Simulated magnetic hysteresis loop for two values of the exchange bias field acting on the pinned nanowire (375 Oe (black) and 250 Oe (red). (c) Simulated domain wall width as a function of the exchange bias field.

We used the OOMMF micromagnetic simulation package[16] to simulate the DWs of the said structure. The LLG equations have been solved with an artificially large damping coefficient of 0.5, since here we are mainly interested in equilibrium magnetization distribution. For the sake of simplification, we consider one structural cell comprising of two nanowires, one pinned nanowire and one unpinned nanowire ferromagnetically coupled to each other. The dimensions of each of the nanowires are 250nm (length)*50nm (width)*5nm (height). In this paper, the exchange bias field is set along the x-axis and the external fields are also applied along the same axis. The cell size for this simulation was 10 nm (length) * 2 nm

(width) * 1 nm (height). We tested even very small cell sizes, such as 5 nm (length) * 0.5 nm (width) * 0.5 nm (height). Fig. 1b shows the magnetization versus field (M-H) loops calculated for exchange bias fields of a pinned Ni nanowire of 375 Oe and 250 Oe. As can be seen in Fig. 1b there are two characteristic fields denoted as H_{n1} (H'_{n1}) and H_{p1} (H'_{p1}). These are characteristic DW fields for the unpinned and pinned nanowires respectively. The H_{n1} (H'_{n1}) field characterizes an onset of incoherent switching or DW formation (nucleation) in the unpinned nanowire. This event is followed by this DW propagation and its penetration into the pinned wire at the characteristic fields H_{p1} (H'_{p1}). It is evident that H_{p1} decreases as H_{xcB} is decreased. Fig. 1c shows the numerically simulated magnetic DW width as a function of the exchange bias field. Clearly, with increased H_{xcB}, DW width is reduced because a higher field is needed to propagate the DW into the pinned nanowire. In this simulation, we used the parameters for Ni: $Ms = 493 \times 10^3 A/m$, $A_0 = 7.2 \times 10^{-12} J/m$, and cubic anisotropy constant $K_1 = -4.5 \times 10^3 J/m^3$. From Fig. 1b we note that all the M-H loops shift to left and the exchange biases calculated from the M-H loops are less than the exchange bias field introduced to the pinned nanowires. This shift originates from strong exchange coupling between wires. For the sake of simplicity, we use the uniform exchange bias field H_{xcB}. The energy of interaction between the neighboring unpinned and pinned magnetoresistive nanowires E_F is defined by the coefficient C_F that is a function of inter-wire exchange coupling strength along the boundary between the adjacent ferromagnetic nanowires. In this particular simulation presented in Fig. 1, $C_F = 1$ meaning that the exchange stiffness along the boundary between magnetoresistive nanowires is the same as inside the nanowires. The inter-wire exchange coupling energy E_F reduces the higher H_{n1} for the higher bias field H_{xcB}. This effect also can be more formally understood for the case H_{p1} using an analogy between considered pinned and unpinned nanowires and a bi-layer of magnetically soft and hard materials. The "hardness" of the pinned wire is controlled by the H_{xcB}. The switching of hard/soft bi-layer has been understood in detail using analytical solutions of 1D problems such as described in Ref. 16. According to this solution, for the case of full inter-wire coupling and the same magnetization for pinned and unpinned wires, one can find the following approximate relation between H_{p1} and H_{xcB}:

$$\mathrm{H_{p1}} \sim \frac{1}{2}\mathrm{H_{xcB}}, \tag{5}$$

This clearly explains why the characteristic field H_{p1} is always found to be visibly smaller than the exchange bias field H_{xcB}. From the Fig. 1, one can see that the DW width decreases with increasing the exchange bias field H_{xcB}. These results can be understood from the conventional DW theory by keeping in mind the analogy between uniaxial anisotropy and exchange bias unidirectional anisotropy. The DW width in Fig.1c was estimated by considering the distribution of magnetization and their projections, i.e., the (M_x) or (M_y) component and using an analytical solution for the Bloch DW. Note, the height of both the nanowires are 5nm. Therefore, the magnetizations are confined in xy plane ($M_z = 0$). The field dependent DW structure for the case of the $H_{xcB} = 1200$ Oe is shown in Fig. 2. The external field is applied along the x-axis and its value is -725 Oe.

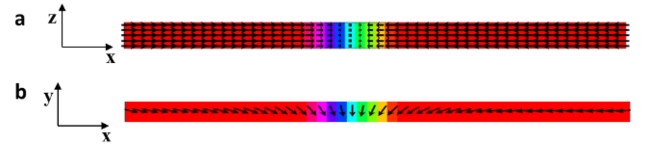

Fig. 2. (a) the field dependence of the magnetization x-component plotted in the zx plane ($y = 125$ nm) for the case of the $H_{xcB} = 1200$ Oe. (b) part of the field dependence of the magnetization plotted in the xy plane ($z = 2$ nm) for the case of the $H_{xcB} = 1200$ Oe. Note, that the colour (dark gray) variation represents the x component of the magnetization.

In order to further understand the DW state, in Fig. 3a, we present the magnetic moment and exchange energy E_{exch} simultaneously as a function of the external field. Fig. 3b shows the magnetization distribution of M_x component along the x-axis for 5 different field positions ($y = 125$ nm). The external field is applied along x-axis and its position is labeled in Fig. 3a. We would like to mention here, in our simulation, we first applied a large field to saturate the magnetization of the nanowires array along the x-axis as for typical MR measurement. In the field position 1, the DW start to nucleate in the unpinned nanowire because of the demagnetization field and anisotropy field. Further decreasing the external field to position 2 (H_{n1}), a DW is formed and its center is in the unpinned nanowire. When the external field reaches $H_{max} = -196$ Oe which is slightly larger than DW nucleation field H_{n1}, the center of the DW will quickly propagate to the boundary which corresponding to the first jump in the

HL loop. Its propagation velocity is proportional to the external field. We can also notice from Fig. 3a that the total magnetization of two nanowires is zero at the field (H_{max} = -196 Oe) at which the exchange energy reaches maximum. Further increasing the external field until the pinning field H_{p1} is reached, up to this point the DW is trapped at the boundary but the center of DW will slightly move to the pinned nanowire. When the external field is larger than the H_{p1} (position 5), the DW will propagate in the pinned nanowire along *x*-axis and then disappear. Therefore, Fig. 3b clearly show that the DW switching mechanism in this case is controlled by the external field. The results also indicate that DW in our case can be controlled by a spin polarized current through spin transfer torque[18].

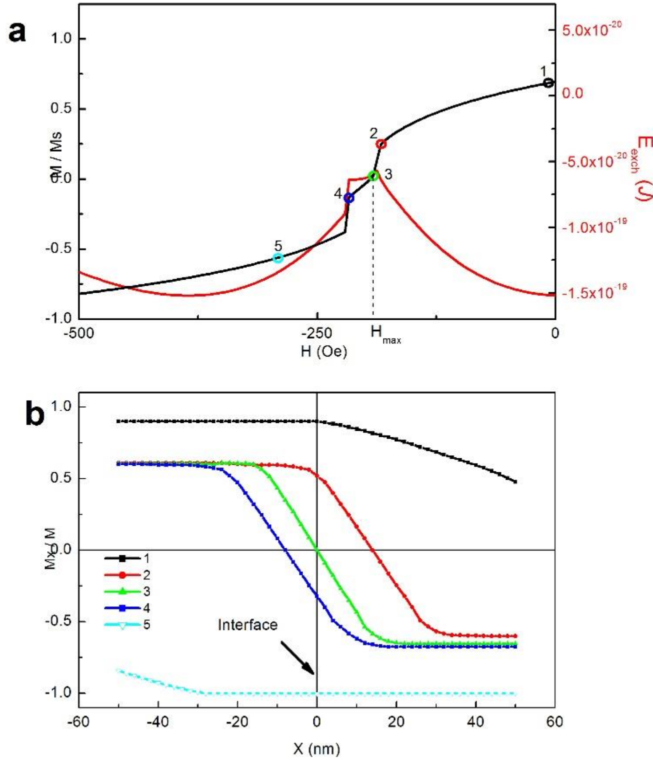

Fig. 3. (a) Simulated magnetic moment (red (dark gray) line) and exchange energy (black line) as a function of external field for the case of the exchange bias field applied to the pinned nanowire H_{xcB} = 375 Oe; (b) the magnetization distribution of M_x component along *x*-axis at 5 different field position (*y* = 125 nm). Note, the external field is applied along *x*-axis and its position is labeled in Fig. 3a.

In order to investigate to what extent the inter-wire exchange interaction between the pinned and unpinned nanowires affects the width of the DW, we calculated the DW width for different values of boundary exchange stiffness. This is important information for the development of magnetic nanowire devices. The prime purpose of spacer nanowires is to reduce exchange coupling between the substrate and the unpinned magnetoresistive nanowires. However, their presence may also modify the boundary exchange stiffness. This reduction should be appreciated by those familiar with epitaxial growth that there is high likelihood of forming a plane of lattice dislocations along the boundary between the pinned and unpinned nanowires, the reason being that the unpinned nanowires grown on the substrate are elevated compared to the pinned nanowires by the thickness of the spacer nanowires. The lattice dislocation can further modify the exchange stiffness along the boundary.

Fig.4 shows the numerically simulated DW width as a function of boundary exchange stiffness. In this simulation, the same parameters for M_s, A_0, and K_1 were used. However, the boundary exchange stiffness A_B varies from 0 to A_0. This means that C_F varies from 0 to 1. The exchange bias field introduced to the pinned Ni nanowire is 375 Oe which is set along the *x*-axis. From the simulation results, we can see that DW width decreases with decreasing boundary exchange stiffness. Decreasing the boundary exchange stiffness decreases the exchange energy and weakens the inter-wire exchange coupling between the neighboring pinned and the unpinned nanowires. We should also point out the close analogy of this reduced inter-wire exchange coupling and studied problem of a hard/soft bi-layer[19]. It has been shown that interfacial exchange coupling strongly affects switching or DW pinning field leading to a characteristic dependence studied both within micromagnetic (numerical and analytical) and atomistic approaches[19].

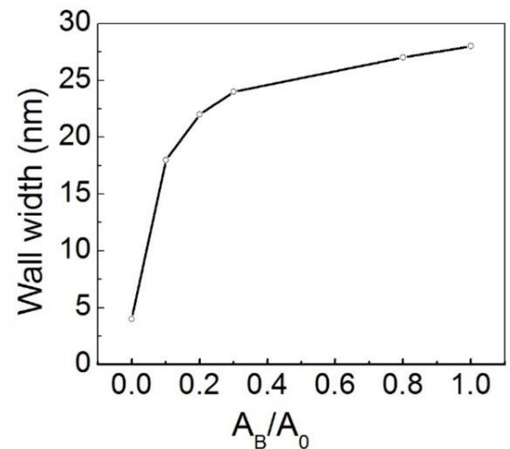

Fig. 4. Simulated domain wall width as a function of the exchange stiffness (J_{AB}) at the pinned unpinend nanowire boundary.

3. Experimental Demonstration

To demonstrate the feasibility of this concept, Fe/Fe_3O_4 nanowire array was grown on *c*-plane sapphire, where Fe nanowire works as the soft material and Fe_3O_4 as the hard material. Fig. 5a shows a schematic drawing of the Fe/Fe_3O_4 nanowire array. The thickness of the Fe and Fe_3O_4 were 1 nm and 20 nm respectively. Details of the growth can be found elsewhere[11,20-22]. Fig. 5b shows an AFM image of the synthesized Fe/Fe_3O_4 nanowire array. Uniform, regular, and straight steps can be clearly observed. Fe_3O_4 is a half-metal with anti-phase boundaries (APBs)[20-34]. For 20 nm thick Fe_3O_4 , the resistivity is typical in the 5×10^{-5} Ohm·m range which is significantly higher than the resistance of Fe, ensuring current will across the interface of Fe and Fe_3O_4 (Marked in Fig. 5a). Fig. 5c shows the magnetoresistance of Fe/Fe_3O_4 nanowire array measured at room temperature. The in-plane magnetic field is applied perpendicular to the steps and from Fe to Fe_3O_4. A MR of -3.7% was achieved at room temperature which is greater than the MR of a flat Fe_3O_4 thin film[33,34] and also greater than the MR of a stepped Fe_3O_4 thin film[35] (Fig. 5d). For flat or stepped Fe_3O_4 thin films, the MR is dominated by transport across the antiferromagnetic APBs. The resistance shows a linear response to the external field at all temperatures and a linear MR is expected[33,34]. However, for the Fe/Fe_3O_4 nanowire array, nonlinear MR is observed, especially in the low field range, indicating a different MR mechanism at low field. Moreover, the MR curve is asymmetric. When the magnetic field is increased from negative to positive (blue curve in Fig. 5c), the resistance decreases rapidly at 260 Oe, suggesting that the DWs propagate from Fe to Fe_3O_4. While when reversing the magnetic field (red curve in Fig. 5c) no such jump is observed.

4. Conclusions

In summary, we investigated parameters controlling nanoscale DW widths in a planar nanowire array with alternating pinned and unpinned wires. A Fe/Fe_3O_4 nanowire array was fabricated to demonstrate the feasibility of this concept and an enhanced MR was observed at room temperature. This information could be useful for the development new spin devices and other applications[36,37].

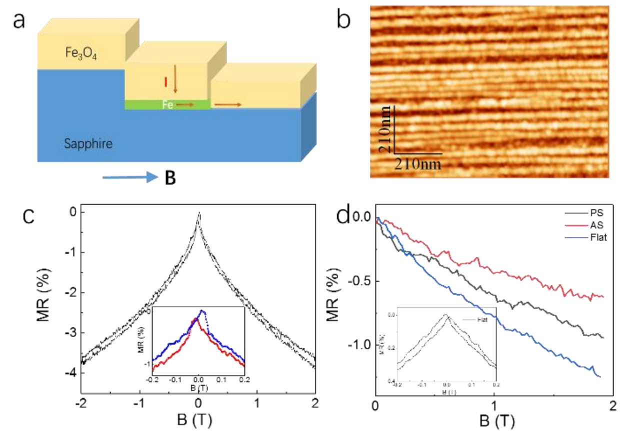

Fig. 5. (a) Schematic drawing of the Fe/Fe_3O_4 nanowire array. (b) AFM image of the Fe/Fe_3O_4 nanowire array. (c) MR of the Fe/Fe_3O_4 nanowire array measured at room temperature. (d) MR of flatted Fe_3O_4 thin film and stepped Fe_3O_4 thin film measured at room temperature, where PS (AS) means current is applied perpendicular (parallel) to steps

Acknowledgments

This work was supported by the National Key R&D Program of China (Grant Nos. 2017YFE0301404 and 2017YFA0303800), the National Natural Science Foundation of China (No. 61874010), and by the Science and Technology Innovation Program for Creative Talents in Beijing Institute of Technology (No. 2017CX01006).

References

1. V.V. Osipov and A.M. Bratkovsky, Appl. Phys. Lett. **84**, 2118 (2004)
2. C.A. Dartora and G.G. Carbera, Phys. Lett. A **334**, 46 (2005)
3. F. Elhoussine, L. Vila, L. Piraux, and G. Faini, J. Magn. Magn, Mater. **290**, 116 (2005)
4. G. G. Cabrera and L. M. Falicov, Phys. Status Solidi B **61**, 539 (1974)
5. H. Imamura, N. Kobayashi, S. Takahashi, and S. Maekawa, Phys. Rev. Lett. **84**, 1003 (2000)
6. L. R. Tagirov, B. P. Vodopyanov, and K. B. Efetov, Phys. Rev. B **65**, 214419 (2002)
7. V. K. Dugaev, J. Berakdar, and J. Barnas, Phys. Rev. B **68**, 104434 (2003)
8. J. J. Mallett, E. B. Svedburg, H. Etteddui, T. P. Moffat, and W. F. Egelhoff, Jr., Phys. Rev. B **70**, 172406 (2004)
9. R. F. Sabirianov, A. K. Solanki, J. D. Burton, S. S. Jaswal, and E. Y. Tsymbal, Phys. Rev. B **72**, 054443 (2005)
10. P. E. Falloon, R. A. Jalabert, D. Weinmann, and R. L. Stamps, Phys. Rev. B **70**, 174424 (2004)

11. I. V. Shvets, H. C. Wu, V. Usov, F. Cuccureddu, S. K. Arora, and S. Murphy, Appl. Phys. Lett. **92**, 023107 (2008)
12. F. Cuccureddu, V. Usov, S. Murphy, C. O. Coileain, and I. V. Shvets, Rev. Sci. Instrum. **79**, 053907 (2008)
13. C. H. Marrows, Adv. Phys. **54**, 585 (2005)
14. O.N. Mryasov, V.A. Gubanov, and A.I. Liechtenstein, Phys. Rev. B **45**, 12330 (1992)
15. L. D. Landau and E. Lifshitz, Phys. Z. Sowjetunion **8**, 153 (1935)
16. M.J. Donahue and D.G. Porter, OOMMF user's guide, version 1.2a. Technical Report NISTIR 6376, National Institute of Standards and Technology, Gaithersburg, MD, (1999)
17. H. Kronmüller and D. Goll, Physica B 319, 122 (2002)
18. J. C. Slonczewski, J. Magn. Magn. Mater. **159**, L1 (1996)
19. K. Y. Guslienko, O. Chubykalo-Fesenko, O. Mryasov, R. W. Chantrell, and D. Weller, Phys. Rev. B **70**, 104405 (2004)
20. S. Arora, H. C. Wu, R. Choudhary, I. Shvets, O. Mryasov, H. Yao, and W. Ching, Phys. Rev. B **77**, 134443 (2008)
21. H. C. Wu, R. Ramos, R. G. S. Sofin, Z. M. Liao, M. Abid, and I. V. Shvets, Appl. Phys. Lett. **101**, 052402 (2012)
22. H. C. Wu, O. N. Mryasov, M. Abid, K. Radican, and I. V. Shvets, Sci. Rep. **3**, 1830 (2013)
23. F. Walz, J. Phys.: Condens. Matter **14**, R285 (2002)
24. M. Ziese, Rep. Prog. Phys. **65**, 143 (2002)
25. J. H. V. J. Brabers, F. Walz and H. Kronmuller, J. Phys.: Condens. Matter. **12**, 5437 (2002)
26. X. Li, A. Gupta, G. Xiao, W. Qian, and V. Dravid, Appl. Phys. Lett. **73**, 3282 (1998)
27. H. C. Wu, S. K. Arora, O. N. Mryasov, and I. V. Shvets, Appl. Phys. Lett. **92**, 182502 (2008)
28. D. T. Margulies, F. T. Parker, M. L. Rudee, F. E. Spada, J. N. Chapman, P. R. Aitchison, and A. E. Berkowitz, Phys. Rev. Lett. **79**, 5162 (1997)
29. D. T. Margulies, F. T. Parker, F. E. Spada, R. S. Goldman, J. Li, R. Sinclair, and A. E. Berkowitz, Phys. Rev. B **53**, 9175 (1996)
30. W. Eerenstein, T. Hibma, S. Celotto, Phys. Rev. B, **70**, 184404 (2004)
31. H.-C. Wu, A. Syrlybekov, O. Mauit, C. Ó Coileáin, A. Mouti, M. Abid, M. Abid, and Igor V. Shvets, Appl. Phys. Lett. **105**, 132408 (2014)
32. A. Syrlybekov, H.-C. Wu, O. Mauit, Y.-C. Wu, P. Maguire, A. Khalid, C. Ó Coileáin, L. Farrell, C.-L. Heng, M. Abid, H. J. Liu, l. Yang, H.-Z. Zhang, and I. V. Shvets, Nanoscale **7**, 14055 (2015)
33. R. G. S. Sofin, Han-Chun Wu, and I. V. Shvets Phys. Rev. B 84, 212403 (2011)
34. H. C. Wu, M. Abid, B. S. Chun, R. Ramos, O. N. Mryasov, and I. V. Shvets, Nano Lett. **10**, 1132 (2010)
35. H.-C. Wu, X. Liu， C. Ó Coileáin, H. Xu, M. Abid, and M. Abid, A. Syrlybekov, O. Mauit, I. V. Shvets, R.G.S. Sofin, J. Cho, B. Sun Chun, and H. Liu, Spin 7, 175001 (2017)
36. X.B. Wang and Y.M. Huai, Spin 7, 1702001 (2017)
37. A. Jabar, R. Masrour. M. Hamedoun, and A. Benyoussef, Spin 7, 1750011 (2017)